International Journal of Nanomedicine

Dovepress
open access to scientific and medical research

Open Access Full Text Article

ORIGINAL RESEARCH

Pterostilbene Nanoparticles Downregulate Hypoxia-Inducible Factors in Hepatoma Cells Under Hypoxic Conditions

This article was published in the following Dove Press journal:
International Journal of Nanomedicine

Wen-Sheng Tzeng[1,2]
Wei-Lin Teng[3]
Pao-Hsien Huang[4]
Tzu-Ching Lin[3]
Feng-Lin Yen[2,5–7]
Yow-Ling Shiue[2]

[1]Department of Radiology, Pingtung Christian Hospital, Pingtung, Taiwan; [2]Institute of Biomedical Sciences, National Sun Yat-Sen University, Kaohsiung, Taiwan; [3]Graduate Institute of Natural Products, College of Pharmacy, Kaohsiung Medical University, Kaohsiung, Taiwan; [4]School of Pharmacy, College of Pharmacy, Kaohsiung Medical University, Kaohsiung, Taiwan; [5]Department of Fragrance and Cosmetic Science, College of Pharmacy, Kaohsiung Medical University, Kaohsiung, Taiwan; [6]Drug Development and Value Creation Research Center, Kaohsiung Medical University, Kaohsiung, Taiwan; [7]Department of Medical Research, Kaohsiung Medical University Hospital, Kaohsiung, Taiwan

Purpose: Transcatheter arterial chemoembolization (TACE) is a common clinical treatment for hepatocellular carcinoma (HCC). However, hypoxia induction after treatment might trigger tumor invasiveness and metastasis. Although pterostilbene (PTS) has antitumor effects, its chemoprevention in HepG2 cells under hypoxia has not been investigated yet. In addition, the poor water solubility of raw PTS limits its clinical application. Here, we prepared nanoparticles of PTS (PSN) and compared their antihepatoma activities with those of raw PTS in HepG2 under hypoxic conditions.

Materials and Methods: The PTS nanoparticle formulation was prepared by nanoprecipitation, using Eudragit® e100 (EE) and polyvinyl alcohol (PVA) as carriers. We analyzed the physicochemical properties of raw PTS and PSN, including yield, encapsulation efficiency, water-solubility, particle size, morphology, crystalline-to-amorphous transformation, and molecular interaction between PTS and carriers. We also evaluated their antihepatoma activities under hypoxia treatment in HepG2 cells, including cell viability, hypoxia, and apoptosis.

Results: The yield and encapsulation efficiency of PSN were 86.33% and >99%, respectively. The water solubility and drug release of PTS were effectively improved after nanoprecipitation corresponding to the reduction in particle size, amorphous transformation, and formation of hydrogen bonding with carriers. PSN had a better cytotoxic effect than raw PTS in HepG2 under pre- and post-hypoxia conditions. In addition, hypoxia- and apoptosis-related proteins in HepG2 cells under two different hypoxic conditions were significantly inhibited by PSN compared with the control group with hypoxia only, except for HIF-1α in the post-hypoxia group. PSN was also significantly better in inhibiting these proteins, except for Bcl2, under pre-hypoxic conditions.

Conclusion: Our results suggested that PSN could improve the water solubility and drug release of PTS and enhance the efficacy of HCC treatment under hypoxic conditions.

Keywords: hepatocellular carcinoma, hypoxia, transcatheter arterial chemoembolization

Correspondence: Feng-Lin Yen
Department of Fragrance and Cosmetic Science, College of Pharmacy, Kaohsiung Medical University, No.100, Shin-Chuan 1st Road, Sanmin Dist., Kaohsiung City, 80708, Taiwan
Tel +886 7 3121101 ext 2028
Email flyen@cc.kmu.edu.tw

Yow-Ling Shiue
Institute of Biomedical Sciences, National Sun Yat-Sen University, No 70 Lien-Hai Road., Kaohsiung City, 80424, Taiwan
Tel +886 7 5252000 ext 5818
Email shirley@imst.nsysu.edu.tw

Introduction

Hepatocellular carcinoma (HCC), one of the primary liver cancers, is known to most often occur in humans with many chronic diseases, including infection with hepatitis B virus (HBV), hepatitis C virus (HCV), nonalcoholic fatty liver disease, metabolic syndrome, diabetes, and obesity.[1] Most patients with liver cancer are diagnosed at a late stage. For patients with unresectable HCC, transarterial chemoembolization (TACE) is considered one of the most effective palliative treatments and has been defined by the Barcelona clinic liver cancer (BCLC) staging

system as a standard treatment for patients with HCC in the intermediate stage.[2,3] However, TACE has been reported to induce tumor hypoxia,[4] resulting in the upregulation of hypoxia-inducible factor-1α (HIF-1α). In a hypoxic environment, HIF-1α is known to stably accumulate and enter the nucleus to promote cancer progression, which might be related to tumor angiogenesis.[4–7] Previous studies have shown that overexpression of HIF-1α led to a reduction in the effectiveness of TACE for HCC.[8] It is well known that overexpression of HIF1α under hypoxia can induce the transcription of cancer metastasis genes, such as Caveolin-1 (CAV-1), and consequently promote the progression of HCC, including migration, invasiveness, and metastasis.[9,10] In addition, overexpression of CAV-1 has been shown to promote the activation of antiapoptotic proteins, such as B-cell lymphoma 2 (BCL2) to inhibit cancer apoptosis and lead to cancer cell survival.[11,12] Therefore, appropriate administration of anticancer drugs during treatment with TACE might improve the rate of recurrence of hypoxia-induced HCC. The TACTICS trial[13] concluded that the combination of TACE plus sorafenib, an oral multikinase inhibitor, could improve the clinical outcomes of TACE in treating unresectable HCC. Nevertheless, the application of sorafenib has been limited by its high cost and frequent adverse events.[13–15]

In recent years, scientists have studied extracts or compounds from natural products, such as plants, marine organisms, and microorganisms. Natural products are known to exhibit fewer side effects, so they can be used as an alternative or adjunct treatment for cancer.[16] One such example is pterostilbene (PTS), which is a natural dimethylated analog of resveratrol, mainly found in *Pterocarpus santalinus, Pterocarpus marsupium*, blueberries, and grapes. In particular, PTS has been reported to exhibit various biological activities, such as antioxidant, antitumor, hypolipidemic, and antidiabetic characteristics, and has been shown to have higher bioavailability than resveratrol.[17–19] Previous research has shown that PTS is cytotoxic in lung, prostate, colon, and liver cancers.[20] Its mechanism of action was that it induced cancer cell death by regulating the cell cycle, apoptosis, and autophagy, concomitantly inhibiting tumor angiogenesis, invasion, and metastasis.[21] However, the molecular biological mechanisms of PTS in hypoxia-induced HCC have not been investigated yet.

Based on our knowledge, approximately 40% of active pharmaceutical ingredients (API) are known to display poor water solubility, which limits their bioavailability.[22] Several limiting physicochemical properties that influence the solubility, bioavailability, and pharmacological effects, are larger particle size, crystalline form, log P, and others. Peng et al revealed that poor water solubility and poor bioavailability of PTS limited its clinical application.[23] It is well known that nanoparticle engineering processes, such as cyclodextrin, micelles, liposomes, polymer nanoparticles, and nanofibers,[24,25] have been used to overcome the poor water solubility and associated limiting physicochemical properties of API and natural products for improving their bioavailability. Eudragit® e100 (EE) is a polymethacrylate copolymer with pH-dependent release characteristics. More specifically, EE is soluble in water with a pH less than 5.5 and does not dissolve in neutral saliva.[25] A previous study showed that microspheres developed with EE extended the drug retention time in the stomach.[26] To date, no one has prepared PTS nanoparticles with EE to overcome the problems of poor water solubility and absorption of PTS.

In this study, we prepared nanoparticle formulations using Eudragit e100 (EE) and polyvinyl alcohol (PVA) by employing nanoprecipitation technology and determined their physicochemical properties to elucidate the mechanism of the potential improvement of their water solubility. The present study demonstrated a novel dosage of PTS nanoparticles (PSN) that could effectively increase the water solubility of raw PTS and improve the anticancer effect in hypoxia-induced HepG2 cells.

Materials and Methods

Preparation of Pterostilbene Nanoparticles

In this study, we used EE (Röhm Pharma, Darmstadt, Germany) as a carrier and particle stabilizer to maintain the homogenization of particles to encapsulate PTS and PVA used as a particle stabilizer. Briefly, PSN with various ratios of PTS:EE:PVA (1:2:2, 1:4:4 and 1:8:8; w/w) were prepared using the nanoprecipitation method,[27] and the process included dissolving EE and PTS in 10 mL ethanol to form an organic solution. The aqueous solution consisted of PVA in 30 mL ultrapure water. Next, the organic solution was slowly injected into the aqueous solution at high speed and homogenized at 22,000 rpm for 5 min. After that, the ethanol in the PSN solution was removed in a rotary evaporator in a 40°C water bath. To remove larger particles, the remaining solution was filtered with a filter paper (Advantec No 1; Toyo Roshi Kaisha, Tokyo, Japan) and a nanoparticle solution (NS) was obtained. Consecutively, we lyophilized the

solution in a freeze dryer for 24 h and placed the dried sample in a humidity control box.

Determination of Size and Morphology of Nanoparticles

PSN sample was diluted 10 times with ultrapure water and immediately placed into a cuvette to measure the mean particle size using a particle size analyzer (ELSZ-2000; Otsuka Electronics, Osaka, Japan). Furthermore, the uniformity of the nanoparticle morphology was observed using a transmission electron microscope (JEOL JEM-2000 EXII TEM; JEOL, Tokyo, Japan). Before the experiment, PSN was stained with 0.5% (w/v) phosphotungstic acid, immediately added it in a carbon-coated copper grid, and then maintained it in a humidity control box with 40% RH (relative humidity) to dry overnight. A scanning electron microscope (SEM; Hitachi S4700, Hitachi, Tokyo, Japan) was used to observe the shape and surface characteristics of PTS and PSN.

Determination of Hydrogen-Bond Formation

The formation of intermolecular hydrogen bonding between PTS and carriers was analyzed with ^{1}H-nuclear magnetic resonance (^{1}H-NMR) and Fourier transform infrared spectroscopy (FT-IR). In brief, we dissolved 5 mg of PTS, PSN with various ratio excipients, and nanocarriers in 0.5 mL of dimethyl sulfoxide-d6 (DMSO-d_6). We evaluated each sample using a Varian Mercury Plus 400 NMR System (Oxford Instrument Co., Oxfordshire, UK). In addition, we determined the functional group involved in the interaction between PTS and the carrier with FT-IR spectroscopy (PerkinElmer 2000 spectrophotometer; PerkinElmer, Norwalk, CT, USA). Subsequently, we uniformly mixed each sample with potassium bromide (KBr) and prepared tablets. The scanning range was set at 400 to 4000 cm^{-1}, and the resolution was set at 1 cm^{-1}.

Crystalline-to-Amorphous Transformation of Pterostilbene, Pterostilbene Nanoparticles, and Nanocarriers

We evaluated the crystalline forms of PTS, PSN with various ratio excipients, and nanocarriers by X-ray diffractometry (XRD) using a Siemens D5000 instrument (Siemens, Munich, Germany). Samples were scanned with Cu-Kα radiation at 40 kV and 25 mA in continuous scan mode. The scanning angle (2θ) was set to a range of 2° to 50° and a scanning rate of 1°/min.

Analysis of Pterostilbene Content in Pterostilbene Nanoparticles by High-Performance Liquid Chromatography

The PTS contents in PSN were determined with an HPLC analysis system (LaChrom Elite L-2000; Hitachi, Tokyo, Japan) and an L-2420 ultraviolet-visible (UV–vis) detector. An HPLC column (Mightysil RP-18 GP column, 250 × 4.6 mm, i.d., 5 μm) was used to analyze the purity of PTS and to prepare a calibration curve of PTS for calculating the concentration of each sample in various studies. The mobile phase was composed of acetonitrile and double-distilled H_2O (35:65, v/v). The flow rate was set at 1.0 mL/min, and the detection wavelength was set at 307 nm. The PTS retention time appeared at about 4.3 min. The correlation coefficient (r) from 0.01 to 50 μg/mL of PTS after HPLC determination was observed to be greater than 0.999, showing a good linear response.

Yield and Encapsulation Efficiency of Pterostilbene Nanoparticles

A good pharmaceutical formulation should display a good yield and encapsulation efficiency in further clinical applications. Briefly, we weighted the PSN sample containing 1 mg PTS, then dissolved it in 1 mL methanol, and immediately analyzed it using the above mentioned HPLC method. The concentration of PTS in PSN after HPLC determination was calculated from the PTS standard curve. The yield of PSN was calculated using the following equation (1):

$$\text{Yield } (\%) = \frac{C_{PSN} \times V_{PSN}}{W_{PTS}} \times 100\% \quad (1)$$

In addition, we determined the encapsulation efficiency of PSN. Each sample was added to a centrifugal filter device (Microcon YM-10; Millipore, Billerica, MA, USA) and centrifuged at 10,000 rpm for 10 min. The unencapsulated PTS was observed to be at the bottom of the tube and then analyzed by HPLC. The encapsulation efficiency of PSN was calculated using the following equation (2):

$$\text{Encapsulation efficiency } (\%) = \frac{C_{PSN} \times V_{PSN} - C_{UPTS} \times V_{PSN}}{C_{PSN} \times V_{PSN}} \quad (2)$$

where C_{PSN} is the concentration of PTS from PSN, V_{PSN} is the volume of PSN, W_{PTS} is the theoretical amount of PTS added, and C_{UPTS} is the concentration of unencapsulated PTS.

Water Solubility of Pterostilbene and Pterostilbene Nanoparticles

1 mg raw PTS and PSN with various ratio excipients (containing 1 mg PTS) were added into 1 mL aqueous

solution (pH 5.5), respectively. And then the mixture was immediately shaken for 5 min. Each sample was passed through a 0.45 μm filter, followed by an analysis of the concentration using an HPLC system.

Cell Viability Assay

The human HCC cell line HepG2 was obtained from the Food Industry Research and Development Institute (Hsinchu, Taiwan) and the HepG2 cells were authenticated by STR profile and its result showed this cell line without any problem. HepG2 cells were cultured in DMEM (Himedia Laboratories, Mumbai, India) supplemented with 10% FBS (Thermo Fisher Scientific, Waltham, MA, USA) and 1% penicillin-streptomycin-amphotericin B solution (PSA; Biological Industries, Cromwell, CT, USA) and maintained in a 37°C incubator with 5% CO_2. First, 1.5×10^4 HepG2 cells were seeded into each well in 96-well plates for 24 h until fully attached. Concomitantly, PTS and PSN were dissolved in water, and a stock solution was prepared, and then passed through a 0.45 μm filter. Subsequently, PTS and PSN were diluted to concentrations of 5 to 80 μM and 0.5 to 8 μM in medium (without FBS), respectively. After incubation, the medium was removed, and different concentrations of PTS and PSN were added to various wells.

Cells were cultured under three different experimental conditions: the control group had normal oxygen supply for 24 h (24N); the pre-hypoxia group was subjected to 6 h of hypoxia followed by normal oxygen supply for 18 h (6H18N); and the post-hypoxia group had normal oxygen supply for 18 h and then was subjected to hypoxia for 6 h (18N6H). After treatment, 150 μL of 0.5% MTT solution was added to each well and incubated for 4 h under normal culture conditions (37° C, 5% CO_2). After that, the MTT medium was removed, and 100 μL of DMSO was added to dissolve the crystals. The absorbance of each well was evaluated at 550 nm using a microplate spectrophotometer (μQuant; Biotek Instruments Inc., Winooski, VT, USA).

Western Blot Analysis

Briefly, 1.5×10^6 HepG2 cells were seeded in a 6-cm dish for 24 h; then, the medium was removed, and cells were washed twice with PBS. Cells were treated with PTS and PSN in FBS-free medium. Cells were cultured under three different conditions: the control group had normal oxygen supply for 12 h; the pre-hypoxia group was subjected to 6 h of hypoxia and then had normal oxygen supply for 6 h, and the post-hypoxia group had normal oxygen supply for 6 h and then subjected to hypoxia for 6 h. After treatment, cells were lysed with RIPA buffer (Millipore) and then centrifuged at 12,000 rpm for 10 min. The protein concentration was determined using the bicinchoninic acid (BCA) protein assay kit (Thermo Fisher Scientific). Samples were separated by 10% SDS–PAGE and then transferred to a PVDF membrane (Millipore). Membranes were blocked for 1 h and then washed with Tris-buffered saline containing 1% Tween-20 (TTBS). Next, membranes were incubated with primary antibodies against HIF-1a (1:1000; Cell Signaling Technology, Danvers, MA, USA), Cav-1 (1:1000; Biosciences, Franklin Lakes, NJ, USA), Cav-3 (1:1000; Abcam, Cambridge, United Kingdom), and Bcl-2 (1:1000; Cell Signaling Technology) at 4°C overnight. Membranes were incubated with an HRP-conjugated secondary antibody for 1 h, and proteins were detected with enhanced chemiluminescence (ECL; Thermo Fisher Scientific) using the ChemiDoc XRS software (BioRad, Hercules, CA, USA).

Statistical Analysis

All data were analyzed using Microsoft Excel 2016 software (Microsoft Office; Microsoft Corporation, Redmond, WA, USA) and the SPSS software version 19 (SPSS Inc., Chicago, IL, USA). Data were expressed as mean ± SD and analyzed by one-way ANOVA with Tukey's test for determination of significant differences. A P-value < 0.05 was considered statistically significant.

Results

Size and Morphology of the Pterostilbene Nanoparticles

The size of particles is related to water solubility because the surface area is known to increase with a reduction in the size, increasing the water solubility. As shown in Table 1, the average size diameter and polydispersity index (PI) of raw PTS were 2816.53 ± 87.00 nm and 1.08 ± 0.02, respectively. In contrast, PSN with the various ratios of the excipients, PTS:EE:PVA (1:2:2, 1:4:4, and 1:8:8; w/w/w) displayed a uniform distribution of nanoparticle sizes. These results indicated that the particle size and PI of PSN decreased in an excipient-dependent manner. We also used transmission electron (TEM) and scanning electron (SEM) microscopy to observe the morphology of PSNs. As shown in the TEM photos in Figure 1A, the PSN particles were in the shape of a sphere, with their particle size consistently being less than 200 nm. In contrast, SEM images showed that raw PTS had an irregular block shape and a particle size

Table 1 Water Solubility, Yield, Encapsulation Efficiency, Particle Size, and PI of PTS and Its Nanoparticle Formulation

PTS:EE:PVA	Water Solubility (μg/mL)	Yield (%)	Encapsulation Efficiency (%)	Particle Size (nm)	PI
1:2:2	158.29 ± 5.65	29.34 ± 5.68	>99	123.53 ± 3.73*	0.22 ± 0.020*
1:4:4	482.49 ± 11.35	79.09 ± 4.63	>99	94.67 ± 0.81*	0.13 ± 0.010*
1:8:8	604.38 ± 49.37	86.33 ± 4.64	>99	102.77 ± 0.49*	0.14 ± 0.004*
PTS	<0.05	ND	ND	2816.53 ± 79.42	1.08 ± 0.020

Notes: Values are mean ± SD (n = 3). *P < 0.05: statistically significant difference compared with PTS.
Abbreviations: PTS, pterostilbene; PSN, PTS nanoparticles; PI, polydispersity index; SD, standard deviation; ND, not detected.

of approximately 10 to 30 μm (Figure 1B). Conversely, PSN was shown to have a thin film shape with a relatively large surface area (Figure 1C). These results showed that PTS nanoparticle formulations had a smaller particle size and larger surface area compared with PTS, resulting in the increased water solubility of raw PTS.

Yield, Encapsulation Efficiency, and Solubility of Raw Pterostilbene and Pterostilbene Nanoparticles

As shown in Table 1, the yield and encapsulation efficiency of PSN were 86.33% and >99%, respectively. The solubility

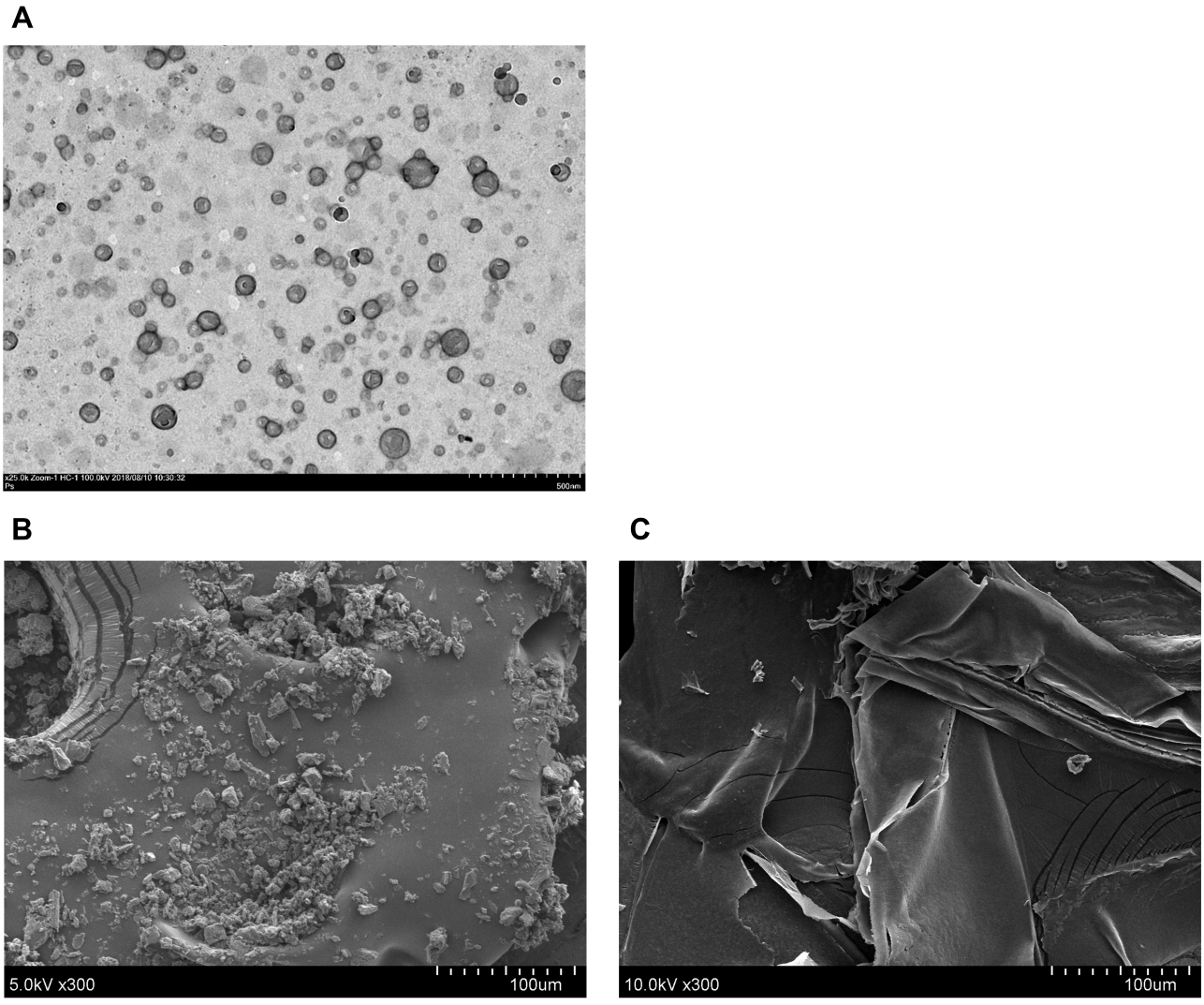

Figure 1 Transmission electron microscopy (TEM) image of PSN (**A**), scanning electron microscopy (SEM) images of raw PTS (**B**) and PSN (**C**).

of PTS and PSN with the various excipient ratios are shown in Table 1. More specifically, PTS was difficult to dissolve in water, and its solubility was below the detected concentration in the calibration curve. This suggested that the water solubility of raw PTS was less than 0.05 μg/mL. In contrast, the water solubility of PSN with the various excipient ratios was shown to be 158.29 ± 5.65, 482.49 ± 11.35 and 604.38 ± 49.37 μg/mL, respectively. These results indicate that the water solubility, yield, particle size reduction, and PI were improved in an excipient-dependent manner. The PTS:EE:PVA ratios of 1:8:8 showed the highest water solubility and yield when compared to other ratios. Therefore, the PTS:EE:PVA ratio at 1:8:8 was the optimal prescription, and we further analyzed its physicochemical properties and antihepatoma activity.

In vitro Drug Release of Pterostilbene Nanoparticles

A good nanoparticle formulation has improved water solubility with a good drug release profile. In vitro studies for drug release of PSN were performed at pH 5.5 and pH 7.4 PBS. Figure 2 shows the in vitro drug release profile of raw PTS and PSN. The drug release percentage of PSN in PBS at pH 5.5 was more than 40% within 120 min, and in PBS at pH 7.4 was less than 2%. PSN at pH 5.5 showed an 80-fold greater drug release than at pH 7.4 due to the Eudragit E100 acid-dependent dissolved polymer and reduced swelling ability above pH 7. In contrast, the drug release percentages of raw PTS at pH 5.5 and PBS at pH 7.4 were also less than 2%. Therefore, the drug release percentages of PSN were significantly higher than those of raw PTS.

Amorphous Transformation of Pterostilbene Nanoparticles

We used XRD to evaluate the transformation of crystalline to amorphous nanometer systems. Amorphous transformation of raw compounds is known to effectively improve water solubility. The XRD graphs of PTS, PSN, and nanocarriers (N) are shown in Figure 3. Several distinct diffraction peaks of PTS in the XRD pattern were shown to be at angles of 19.3°, 23.4°, and 25.5°, indicating PTS as a crystalline compound. In contrast, we did not observe any characteristic peaks of PTS in the XRD pattern of PSN. These results indicated that the PSN prepared with EE and PVA by nanoprecipitation effectively changed the crystalline to an amorphous form, which is considered a mechanism of improvement in the water solubility of PSN.

Pterostilbene Interacted with Nanocarriers by Hydrogen Bonding

Fourier-transform infrared spectroscopy (FT-IR) and proton nuclear magnetic resonance (^{1}H-NMR) are often used to assess the formation of hydrogen bonds between drugs and nanocarriers. In Figure 4A, the FT-IR spectrum of raw PTS showed the characteristic absorption of phenolic–OH stretching at 3348 cm^{-1}, aromatic rings C=C at 1594 cm^{-1},

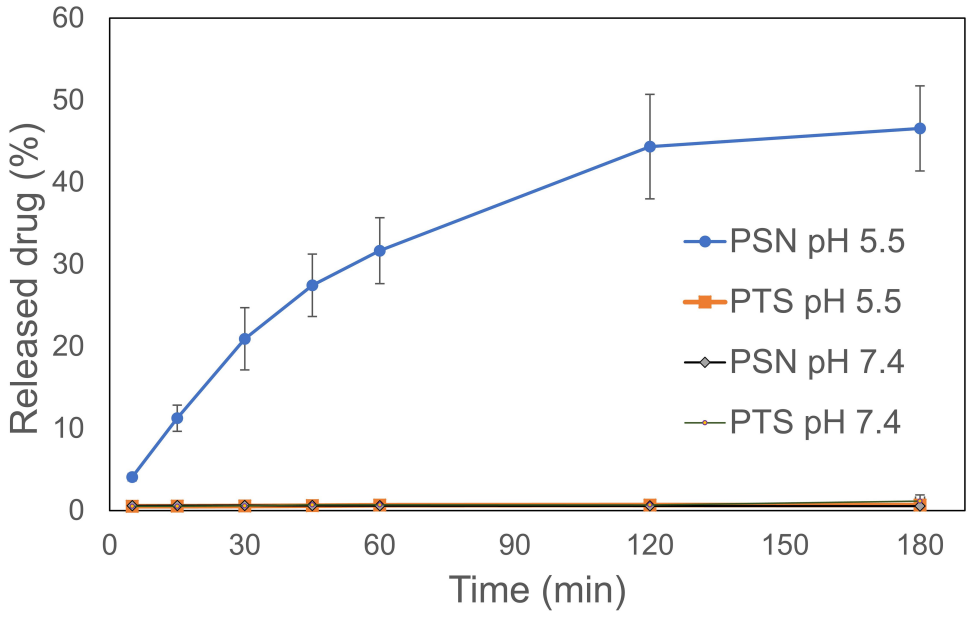

Figure 2 In vitro drug release profiles of raw PTS and PSN in two phosphate buffer solutions.

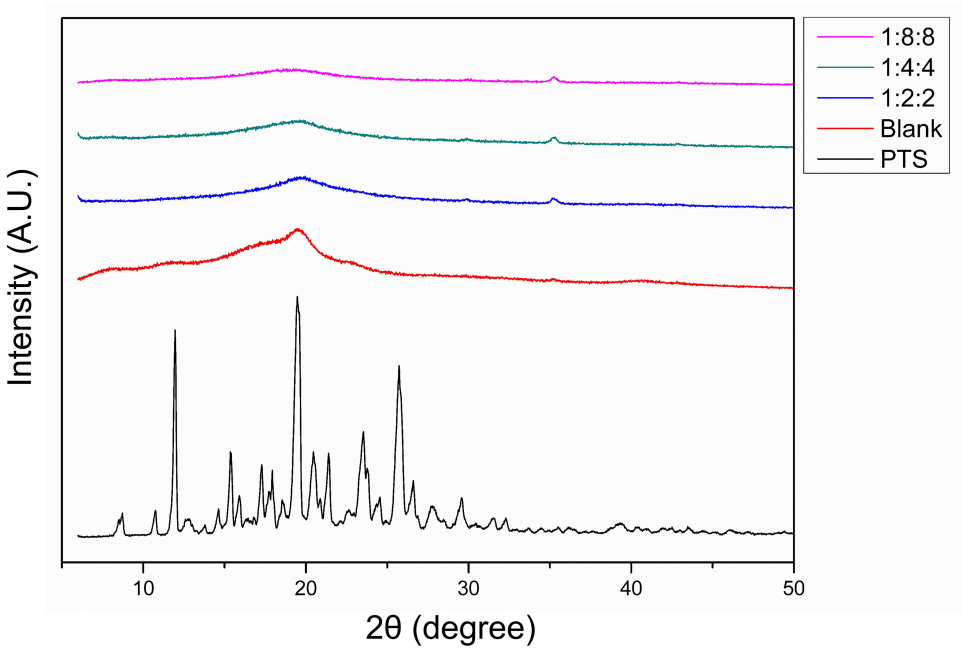

Figure 3 Crystalline and amorphous transformation using powder XRD analysis. The ratio represents the content of PTS:EE:PVA in PSN and the Blank represents only EE and PVA.

C-O-H stretching at 1202 cm^{-1}, and -C-O- stretching vibration at 1356 cm^{-1}. The N spectrum revealed the absorption of the dimethylamino group at 2824 cm^{-1} and 2772 cm^{-1}. In contrast, the spectrum of PSN showed that phenolic–OH stretching had shifted to 3408 cm^{-1}, displaying a broad band. In addition, we did not observe C-O-H stretching at 1202 cm^{-1} and the dimethylamino group at 2824 cm^{-1} in the spectrum of PSN. These results implied that PTS was loaded in the EE and PVA groups after the formulation of nanoparticles.

We also investigated the hydro-binding of PTS and nanocarriers using ^{1}H-NMR spectra (Figure 4B–F). We observed several characteristic protons in the PTS ^{1}H-NMR spectra, such as aromatic protons in the regions of δ6.3–7.5 ppm, methyl protons at δ3.8, and hydroxyl protons at δ9.6 (Figure 4B). In addition, Figure 4 shows that the integrated intensity at δ9.6 ppm of PTS was observed in PSN with excipient ratios of 1:2:2 (Figure 4D) and 1:4:4 (Figure 4E); however, PSN with a 1:8:8 excipient ratio did not display an integrated signal (Figure 4F). Moreover, we observed that in the spectrum of PSN that had an excipient ratio of 1:8:8, these protons had shifted and the hydroxyl proton had disappeared (Table 2 and Figure 5). These results demonstrated that EE100/PVA effectively encapsulated PTS via intermolecular hydrogen-bonding and formed a stable nanoparticle formulation.

Time Point of the Expression of HIF-1a Protein and the Effect of Pterostilbene and Pterostilbene Nanoparticles on Cell Viability in Human HepG2 Hepatocellular Carcinoma Cells Under Hypoxia

Hypoxia-inducible factor 1-α (HIF-1α) is an indicator protein of cells under hypoxia and one of the main factors for poor prognosis of TACE. Therefore, we analyzed the expression levels of the HIF-1α protein at different time points. As shown in Figure 6A, compared with the control group (normoxia), HepG2 cells showed the highest expression of the HIF-1α protein after hypoxia for 6 h, which returned to the same levels as the control group at 48 h. Thus, we used the 6-h hypoxia time point of HepG2 cells as the hypoxia-inducing condition in subsequent experiments.

To determine whether the nanoparticle formulation of PTS could effectively improve the biological activity of PTS, we evaluated the antihepatoma activity of PTS and PSN in the HepG2 cell line. As shown in Figure 6B, raw PTS dissolved in KH_2PO_4 buffer solution did not affect cell viability in the control (24N) and post-hypoxia (18N6H) groups. A slight toxicity was observed in the pre-hypoxia group (6H18N), which was not significantly different ($P > 0.05$). Figure 6C shows that PSN significantly

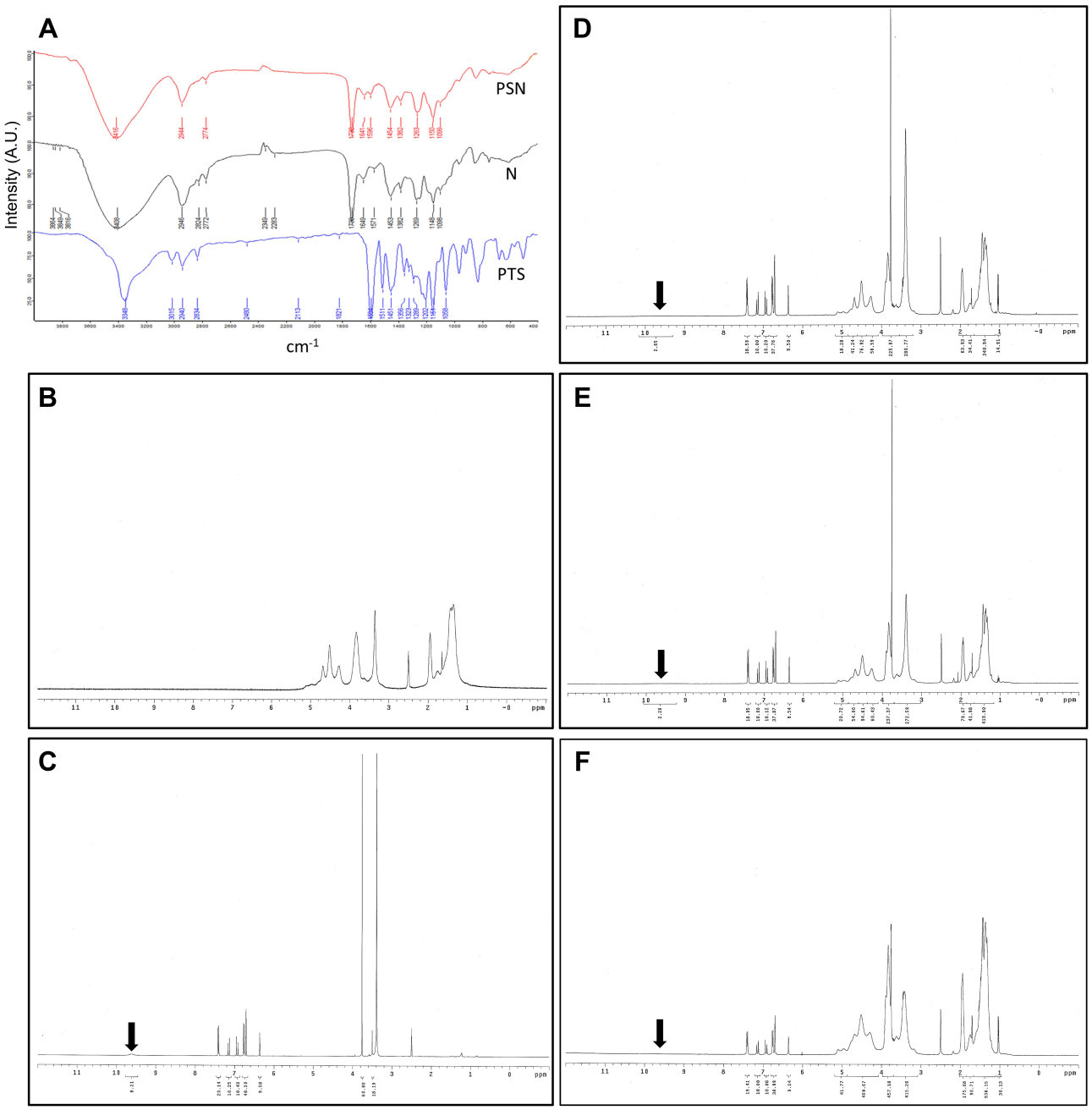

Figure 4 Analysis of hydrogen bonding interactions. FT-IR (**A**) and ^{1}H NMR (**B**–**F**); (**B**) nanoparticle carrier, (**C**) PTS, (**D**) PSN1:2:2, (**E**) PSN1:4:4, (**F**) PSN1:8:8. The direction of the arrows represents the position of the hydrogen bond between PTS and EE-PVA.

reduced cell viability under normoxia and all hypoxia conditions in a dose-dependent manner ($P < 0.05$). In addition, PSN was demonstrated to inhibit about 50% cell viability at 4 μM. In contrast, PTS did not affect cell viability at the same concentration; and even 40 μM PTS did not produce any significant effect. These results indicated that the PTS nanoparticle formulation in buffer solution showed a better antiproliferation effect in HepG2 cells than raw PTS.

Hypoxia and Inhibition of Antiapoptotic Proteins by Pterostilbene Nanoparticles

To understand the molecular mechanism of nanoparticle formulation of PTS under hypoxic conditions, we used Western blot analysis to determine the expression of hypoxia proteins in HepG2 cells after treatment with PTS or PSN. As shown in Figure 7, expression of HIF-1α protein showed a slight increase in both hypoxia groups

Table 2 400 MHz ^{1}H Chemical Shift (δ, ppm) of PTS Protons in Raw State and Chemical Shift Displacements (Δδ, ppm) of PTS Prepared by EE and PVA

Proton Position	δ_{PTS}	With Nanocarrier	
		δ_{PSN}	Δδ
H_a	6.364	6.357	−0.007
H_b	6.712	6.701	−0.011
H_c	7.131	7.121	−0.010
H_d	6.914	6.905	−0.009
H_e	7.422	7.392	−0.030
H_f	6.770	6.750	−0.020
Methyl	3.761	3.758	−0.003
Hydroxyl	9.617	ND	ND

Abbreviations: ND, not detected; Δδ, δ_{PSN} -δ_{PTS}.

(pre-hypoxia and post-hypoxia), despite no significant difference. In addition, we observed significant induction of the expression of CAV-3 and BCL2 proteins in both hypoxia groups and that of CAV-1 in the pre-hypoxia group (Figure 7B). Compared with that in the control under hypoxic conditions, treatment of HepG2 cells with PSN significantly inhibited the protein expression of CAV-1, CAV-3, and BCL2 in both hypoxia groups, as well as that of HIF-1α in the pre-hypoxia group (Figure 7B). In contrast, treatment of HepG2 cells with PTS did not significantly inhibit the expression of the aforementioned proteins, except for CAV-3 in the pre-hypoxia group (Figure 7B). The expression of all four proteins was lower in cells treated with PSN compared with that in cells treated with PTS, with significant differences observed in both hypoxia groups, except for BCL-2 in the pre-hypoxia group (Figure 7B). These results showed that, under post-hypoxia or pre-hypoxia conditions, the PTS nanoparticle formulation effectively improved the suppression of the expression of hypoxic and antiapoptotic proteins.

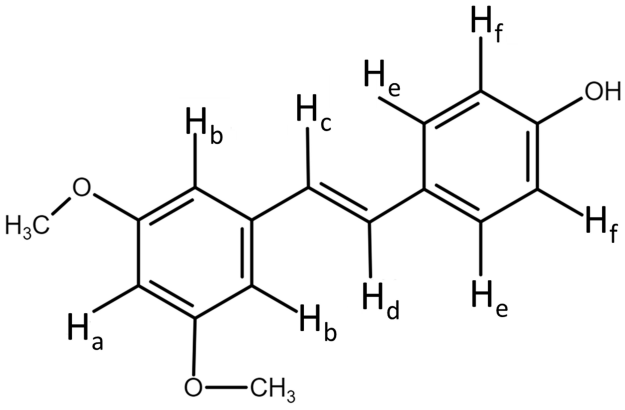

Figure 5 Chemical structure of pterostilbene.

Discussion

The stilbene family, which includes compounds such as pterostilbene, is known to exist in many plants, and its members have been reported to exhibit antioxidant, anti-inflammatory, chemopreventive, and anticancer properties.[28] However, the pharmacological activity of PTS in vitro or in vivo has been limited by its poor water solubility arising from its physicochemical properties.[29] Nanoparticle formulations could improve the water solubility of small-molecule compounds, such as hydrophobic flavonoids[30] and isoflavone.[31] In our study, PSN prepared using EE and PVA were shown to improve the water solubility and drug release of PTS by reducing the particle size, inducing an amorphous transformation, and leading to the formation of hydrogen bonds with nanocarriers. In addition, PSN had a better dissolution profile in PBS at pH 5.5 but not at pH 7.4. These results indicated that PSN can escape the dissolution of the oral solution (pH 7.4), can be quickly dissolved in the intestinal solution (pH 5.5), and may be present the absorption enhancement in intestinal. PSN improved the antihepatoma activity of raw PTS in a buffer solution under hypoxic conditions. Furthermore, we also confirmed that PSN inhibited the growth of HepG2 cells by reducing the expression of hypoxia and antiapoptotic proteins.

Many studies in the past have demonstrated that reducing the size of particles would increase solubility, increase surface area, and reduce the diffusion layer, as well as increase bioavailability.[32] Our TEM and particle size analyzer experiments revealed that PSN had a spherical shape, with particle size less than 200 nm, which was reduced by 17.5 times compared with that of raw PTS. In addition, our SEM results showed that the change in the PSN morphology increased the surface area compared with that of raw PTS. These results indicated that the PTS nanoparticle formulations reduced the size of the particles and increased the surface area, thus increasing the water solubility of PTS by more than 12,000 times. Mora-Huertas et al proposed that the yield and encapsulation efficiency would affect the release and absorption of nanoparticles.[33] In our study, the yield and encapsulation efficiency of PSN was demonstrated to be 86.33% and >99%, respectively. This finding indicated that PSN has a good yield and encapsulation efficiency. Solid-phase drugs can be distinguished as being in either a crystalline

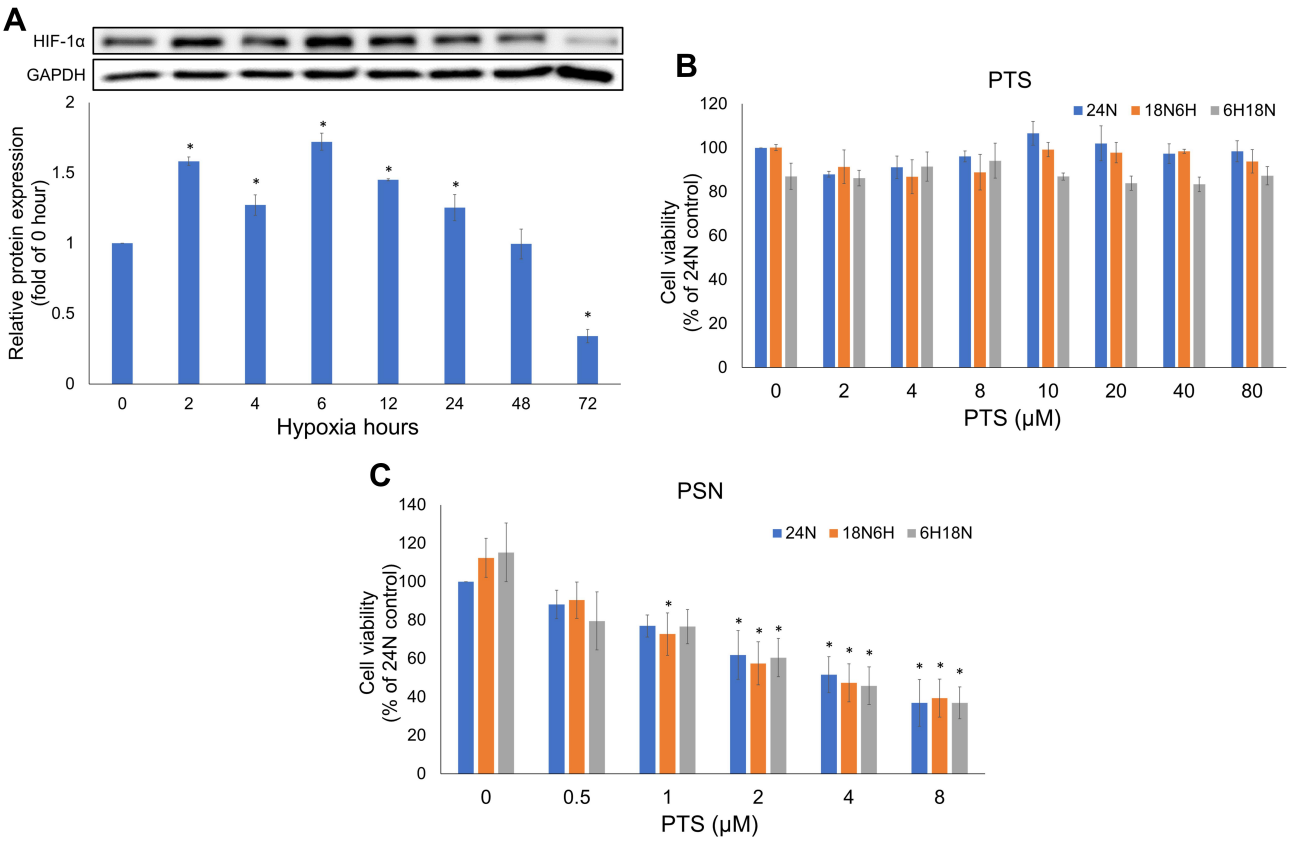

Figure 6 Expression of HIF-1α protein at different time points after hypoxia, and viability of HepG2 cells treated with PTS and PSN for 24 h. Viability of HepG2 cells and expression of HIF-1α protein (**A**). Cell viability following treatment with PTS (**B**) and PSN (**C**) under all hypoxia conditions. n = 3 of each group; *P < 0.05 compared with control.

or amorphous state. Among them, amorphous solids have been reported to have higher thermodynamic energy, resulting in them exhibiting higher solubility and dissolution rates than crystalline solids. Therefore, conversion of a crystalline drug into an amorphous form could improve its water solubility.[34] As shown in Figure 3, EE- and PVA-encapsulated PTS changed the crystalline nature of raw PTS to the amorphous form. Additionally, it is well known that the formation of hydrogen bonds between nanocarriers and lipophilic bioactive compounds could effectively enhance the water solubility of the raw compound.[35] According to our results, the PTS phenolic–OH was shifted to a higher wavenumber in the FT-IR spectrum of PSN. In addition, the spectrum of the dimethylamino group and phenolic proton disappeared in PSN. Previous studies have indicated that hydrophobic drugs can increase water solubility by forming hydrogen bonds with polymers.[27,36] Accordingly, in the PSN with the highest excipient ratio spectrum (Figure 4D), we observed that almost all protons showed an upfield shift (Table 2 and Figure 5), while the hydroxyl proton signal disappeared, representing the interaction between PTS and EE-PVA. An appropriate explanation may be that PTS was successfully encapsulated into excipients after the nanoparticle preparation process, and our results showed that PSN can increase the water solubility of PTS and the yield of PSN in an excipient weight ratio dependent manner. These results indicated that the higher ratio excipient was effectively encapsulated the PTS and subsequently formed more PSN relative to lower ratio excipients. Therefore, we hypothesized that the improvement in water solubility of PTS was accomplished through the encapsulation of PTS with EE and PVA and the formation of hydrogen bonds.

PTS could inhibit the proliferation of HepG2 cells by regulating the p53/SOD2 pathway to increase the intracellular levels of reactive oxygen species (ROS) and lead to activation of the mitochondrial apoptotic pathway.[37] However, no studies have suggested that PTS inhibits the growth of HCC cells under hypoxia by inhibiting HIF-1α. Despite the promising results of the TACTICS trial,[13] all five randomized controlled trials testing combinations of TACE with molecular targeted agents, including sorafenib,

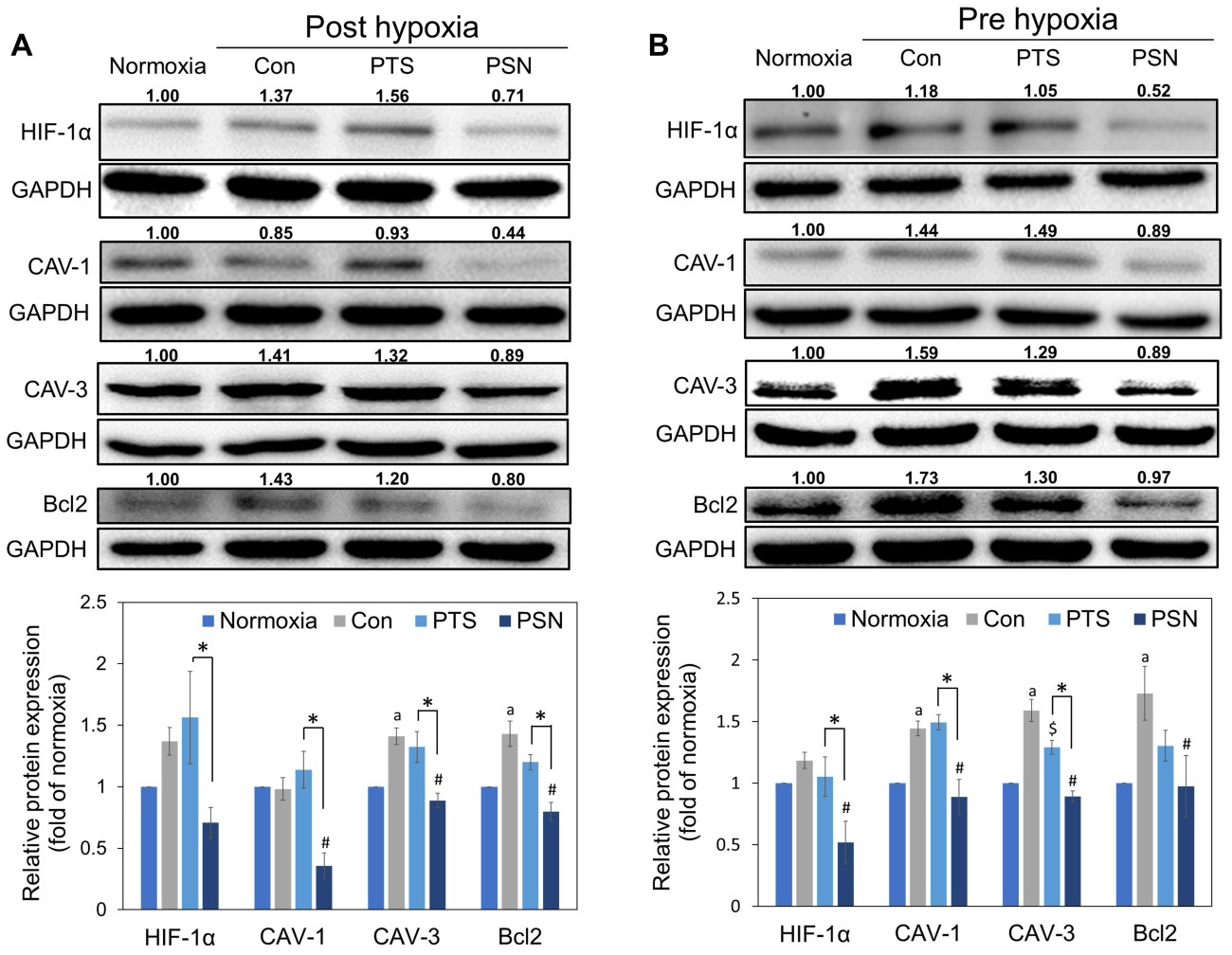

Figure 7 Expression of hypoxia-induced and antiapoptotic proteins post-hypoxia (**A**) and pre-hypoxia (**B**). Protein was collected after treatment of HepG2 cells with 40 μM PTS or PSN containing 4 μM PTS. Protein expression was determined by Western blotting. Columns represent mean ± standard deviation (n = 3). $P < 0.05$: [a]Normoxia compared with control; [$]PTS compared with control; [#]PSN compared with control; *PTS compared with PSN.

brivanib, and orantinib, failed to show the clinical benefits of these combinations. Kudo et al compared the study protocols of these trials and concluded that the improved outcomes observed in the TACTICS trial might be due to the much longer administration of sorafenib, which was given 2–3 wk before the initiation of TACE.[38–43] Therefore, we established two HepG2 hypoxia modes: pre- and post-hypoxia according to the different timings of administration of study drugs, before or after hypoxia, to simulate the conditions of the TACTICS trial in our evaluation of the effect of PTS and PSN on HepG2 cells under hypoxia. The current results showed that PSN significantly reduced the hypoxia-induced expression of the HIF-1α protein. Both caveolin 1 (CAV-1) and CAV-3 are members of caveolins, a scaffolding protein family, and are known to have a similar structure and function.[44,45] For instance, CAV-1 has been reported to be overexpressed in highly metastatic HCC, enhancing the invasive and metastatic potentials of HCC through the induced transcription of HIF-1α under hypoxia.[9,10,46] The expression level of the CAV-3 protein was shown to be significantly upregulated in hypoxic cardiomyocytes;[47] however, its relationship with hypoxic cancer cells has not yet been reported. In our study, CAV-1 and CAV-3 were found to be significantly inhibited by PSN (Figure 7), regardless of pre-hypoxia or post-hypoxia conditions. In addition, the expression of the BCL-2 antiapoptotic protein was demonstrated to be inhibited by PSN. We could thus conclude that PSN exhibited antiproliferative activity in HepG2 cells. In contrast, PTS did not inhibit the expression of any of the aforementioned hypoxia-induced proteins. These results demonstrated that PSN significantly improved the PTS-stimulated inhibition of hypoxia and expression of antiapoptotic proteins and inhibited the proliferation of HepG2 cells.

Conclusion

In conclusion, we prepared a stable PTS nanoparticle formulation using EE and PVA and elucidated the mechanism of improvement of its water solubility and in vitro drug release. We also demonstrated that PSN could reduce the proliferation of HepG2 cells by inhibiting the expression of hypoxia-induced and antiapoptotic proteins, including HIF-1α, CAV-1, CAV-3, and BCL-2. Accordingly, PSN could be an adjuvant in the treatment of HCC, especially in the improvement of prognosis of patients treated with TACE.

Acknowledgments

The authors thank Professor Chih-Hua Tseng who provided pterostilbene and chemical analysis. We also thank Shang-Yi Lin and Li-Hsiang Chen for their supports in data management and statistical analysis. We also thank Mrs. Shui-Chin Lu for the technical support (Center for Research Resources and Development at Kaohsiung Medical University).

Author Contributions

WST, FLY, and YLS made substantial contributions to the conception and design of the study. WLT, TCL, and PHH acquired and analyzed the data. WST, FLY, and WLT interpreted the data and helped draft the manuscript. All authors substantially revised the manuscript for intellectual content. All authors agreed to submit the manuscript to the current journal, gave final approval for the version to be published, and agree to be accountable for all aspects of the work.

Funding

This research was supported by the annual research project of Pingtung Christian Hospital (NO. PS107009).

Disclosure

The authors report no conflicts of interest in this work.

References

1. Forner A, Reig M, Bruix J. Hepatocellular carcinoma. *Lancet*. 2018;391:1301–1314. doi:10.1016/S0140-6736(18)30010-2
2. Song DS, Nam SW, Bae SH, et al. Outcome of transarterial chemoembolization-based multi-modal treatment in patients with unresectable hepatocellular carcinoma. *World J Gastroenterol*. 2015;21:2395–2404. doi:10.3748/wjg.v21.i8.2395
3. Han K, Kim JH. Transarterial chemoembolization in hepatocellular carcinoma treatment: Barcelona clinic liver cancer staging system. *World J Gastroenterol*. 2015;21:10327–10335. doi:10.3748/wjg.v21.i36.10327
4. Lin D, Wu J. Hypoxia inducible factor in hepatocellular carcinoma: a therapeutic target. *World J Gastroenterol*. 2015;21:12171–12178. doi:10.3748/wjg.v21.i42.12171
5. Li X, Feng GS, Zheng CS, Zhuo CK, Liu X. Expression of plasma vascular endothelial growth factor in patients with hepatocellular carcinoma and effect of transcatheter arterial chemoembolization therapy on plasma vascular endothelial growth factor level. *World J Gastroenterol*. 2004;10:2878–2882. doi:10.3748/wjg.v10.i19.2878
6. Carmeliet P, Jain RK. Angiogenesis in cancer and other diseases. *Nature*. 2000;407:249–257. doi:10.1038/35025220
7. Wang B, Xu H, Gao ZQ, Ning HF, Sun YQ, Cao GW. Increased expression of vascular endothelial growth factor in hepatocellular carcinoma after transcatheter arterial chemoembolization. *Acta Radiol*. 2008;49:523–529. doi:10.1080/02841850801958890
8. Liu K, Min XL, Peng J, Yang K, Yang L, Zhang XM. The changes of HIF-1alpha and VEGF expression after TACE in patients with hepatocellular carcinoma. *J Clin Med Res*. 2016;8:297–302. doi:10.14740/jocmr2496w
9. Liu WR, Jin L, Tian MX, et al. Caveolin-1 promotes tumor growth and metastasis via autophagy inhibition in hepatocellular carcinoma. *Clin Res Hepatol Gastroenterol*. 2016;40:169–178. doi:10.1016/j.clinre.2015.06.017
10. Mao X, Wong SY, Tse EY, et al. Mechanisms through which hypoxia-induced caveolin-1 drives tumorigenesis and metastasis in hepatocellular carcinoma. *Cancer Res*. 2016;76:7242–7253. doi:10.1158/0008-5472.CAN-16-1031
11. Edlich F. BCL-2 proteins and apoptosis: recent insights and unknowns. *Biochem Biophys Res Commun*. 2018;500:26–34. doi:10.1016/j.bbrc.2017.06.190
12. Shajahan AN, Dobbin ZC, Hickman FE, Dakshanamurthy S, Clarke R. Tyrosine-phosphorylated caveolin-1 (Tyr-14) increases sensitivity to paclitaxel by inhibiting BCL2 and BCLxL proteins via c-Jun N-terminal kinase (JNK). *J Biol Chem*. 2012;287:17682–17692. doi:10.1074/jbc.M111.304022
13. Kudo M, Ueshima K, Ikeda M, et al.; group, T. s. Randomised, multicentre prospective trial of transarterial chemoembolisation (TACE) plus sorafenib as compared with TACE alone in patients with hepatocellular carcinoma: TACTICS trial. *Gut*. 2020;69:1492–1501. doi:10.1136/gutjnl-2019-318934.
14. Pinter M, Hucke F, Graziadei I, et al. Advanced-stage hepatocellular carcinoma: transarterial chemoembolization versus sorafenib. *Radiology*. 2012;263:590–599. doi:10.1148/radiol.12111550
15. Llovet JM, Ricci S, Mazzaferro V, et al. Sorafenib in advanced hepatocellular carcinoma. *N Engl J Med*. 2008;359:378–390. doi:10.1056/NEJMoa0708857
16. Liao CY, Lee CC, Tsai CC, et al. Novel investigations of flavonoids as chemopreventive agents for hepatocellular carcinoma. *Biomed Res Int*. 2015;2015:840542. doi:10.1155/2015/840542
17. Estrela JM, Ortega A, Mena S, Rodriguez ML, Asensi M. Pterostilbene: biomedical applications. *Crit Rev Clin Lab Sci*. 2013;50:65–78. doi:10.3109/10408363.2013.805182
18. Chen RJ, Kuo HC, Cheng LH, et al. Apoptotic and nonapoptotic activities of pterostilbene against cancer. *Int J Mol Sci*. 2018;19. doi:10.3390/ijms19010287.
19. Lee PS, Chiou YS, Ho CT, Pan MH. Chemoprevention by resveratrol and pterostilbene: targeting on epigenetic regulation. *Biofactors*. 2018;44:26–35. doi:10.1002/biof.1401
20. Yu CL, Yang SF, Hung TW, Lin CL, Hsieh YH, Chiou HL. Inhibition of eIF2alpha dephosphorylation accelerates pterostilbene-induced cell death in human hepatocellular carcinoma cells in an ER stress and autophagy-dependent manner. *Cell Death Dis*. 2019;10:418. doi:10.1038/s41419-019-1639-5
21. Lin WS, Leland JV, Ho CT, Pan MH. Occurrence, bioavailability, anti-inflammatory, and anticancer effects of pterostilbene. *J Agric Food Chem*. 2020. doi:10.1021/acs.jafc.9b07860

22. Savjani KT, Gajjar AK, Savjani JK. Drug solubility: importance and enhancement techniques. *ISRN Pharm*. 2012;2012:195727. doi:10.5402/2012/195727
23. Peng RM, Lin GR, Ting Y, Hu JY. Oral delivery system enhanced the bioavailability of stilbenes: resveratrol and pterostilbene. *Biofactors*. 2018;44:5–15. doi:10.1002/biof.1405
24. Summerlin N, Soo E, Thakur S, Qu Z, Jambhrunkar S, Popat A. Resveratrol nanoformulations: challenges and opportunities. *Int J Pharm*. 2015;479:282–290. doi:10.1016/j.ijpharm.2015.01.003
25. Roberts MS, Mohammed Y, Pastore MN, et al. Topical and cutaneous delivery using nanosystems. *J Control Release*. 2017;247:86–105. doi:10.1016/j.jconrel.2016.12.022
26. Singh V, Chaudhary AK. Preparation of Eudragit E100 microspheres by modified solvent evaporation method. *Acta Pol Pharm*. 2011;68:975–980.
27. Huang PH, Hu SC, Lee CW, Yeh AC, Tseng CH, Yen FL. Design of acid-responsive polymeric nanoparticles for 7,3′,4′-trihydroxyisoflavone topical administration. *Int J Nanomedicine*. 2016;11:1615–1627. doi:10.2147/IJN.S100418
28. Lee YH, Chen YY, Yeh YL, Wang YJ, Chen RJ. Stilbene compounds inhibit tumor growth by the induction of cellular senescence and the inhibition of telomerase activity. *Int J Mol Sci*. 2019;20. doi:10.3390/ijms20112716.
29. Wang P, Sang S. Metabolism and pharmacokinetics of resveratrol and pterostilbene. *Biofactors*. 2018;44:16–25. doi:10.1002/biof.1410
30. Hsu W-C, Ng L-T, Wu T-H, Lin L-T, Yen F-L, Lin -C-C. Characteristics and antioxidant activities of silymarin nanoparticles. *J Nanosci Nanotechnol*. 2012;12(3):2022–2027. doi:10.1166/jnn.2012.5173
31. Huang PH, Hu SCS, Yen FL, Tseng CH. Improvement of skin penetration, antipollutant activity and skin hydration of 7,3′,4′-trihydroxyisoflavone cyclodextrin inclusion complex. *Pharmaceutics*. 2019;11:399. doi:10.3390/pharmaceutics11080399
32. Sun J, Wang F, Sui Y, et al. Effect of particle size on solubility, dissolution rate, and oral bioavailability: evaluation using coenzyme Q(1)(0) as naked nanocrystals. *Int J Nanomedicine*. 2012;7:5733–5744. doi:10.2147/IJN.S34365
33. Mora-Huertas CE, Fessi H, Elaissari A. Polymer-based nanocapsules for drug delivery. *Int J Pharm*. 2010;385:113–142. doi:10.1016/j.ijpharm.2009.10.018
34. An JH, Lim C, Kiyonga AN, et al. Co-amorphous screening for the solubility enhancement of poorly water-soluble mirabegron and investigation of their intermolecular interactions and dissolution behaviors. *Pharmaceutics*. 2018;10:149. doi:10.3390/pharmaceutics10030149
35. Li B, Wen M, Li W, He M, Yang X, Li S. Preparation and characterization of baicalin-poly -vinylpyrrolidone coprecipitate. *Int J Pharm*. 2011;408:91–96. doi:10.1016/j.ijpharm.2011.01.055
36. Khutoryanskiy VV. Hydrogen-bonded interpolymer complexes as materials for pharmaceutical applications. *Int J Pharm*. 2007;334:15–26. doi:10.1016/j.ijpharm.2007.01.037
37. Guo L, Tan K, Wang H, Zhang X. Pterostilbene inhibits hepatocellular carcinoma through p53/SOD2/ROS-mediated mitochondrial apoptosis. *Oncol Rep*. 2016;36:3233–3240. doi:10.3892/or.2016.5151
38. Kudo M, Imanaka K, Chida N, et al. Phase III study of sorafenib after transarterial chemoembolisation in Japanese and Korean patients with unresectable hepatocellular carcinoma. *Eur J Cancer*. 2011;47:2117–2127. doi:10.1016/j.ejca.2011.05.007
39. Lencioni R, Llovet JM, Han G, et al. Sorafenib or placebo plus TACE with doxorubicin-eluting beads for intermediate stage HCC: the SPACE trial. *J Hepatol*. 2016;64:1090–1098. doi:10.1016/j.jhep.2016.01.012
40. Meyer T, Fox R, Ma YT, et al. Sorafenib in combination with transarterial chemoembolisation in patients with unresectable hepatocellular carcinoma (TACE 2): a randomised placebo-controlled, double-blind, Phase 3 trial. *Lancet Gastroenterol Hepatol*. 2017;2:565–575. doi:10.1016/S2468-1253(17)30156-5
41. Kudo M, Han G, Finn RS, et al. Brivanib as adjuvant therapy to transarterial chemoembolization in patients with hepatocellular carcinoma: a randomized phase III trial. *Hepatology*. 2014;60:1697–1707. doi:10.1002/hep.27290
42. Kudo M, Cheng AL, Park JW, et al. Orantinib versus placebo combined with transcatheter arterial chemoembolisation in patients with unresectable hepatocellular carcinoma (ORIENTAL): a randomised, double-blind, placebo-controlled, multicentre, phase 3 study. *Lancet Gastroenterol Hepatol*. 2018;3:37–46. doi:10.1016/S2468-1253(17)30290-X
43. Kudo M, Arizumi T. Transarterial chemoembolization in combination with a molecular targeted agent: lessons learned from negative trials (Post-TACE, BRISK-TA, SPACE, ORIENTAL, and TACE-2). *Oncology*. 2017;93(Suppl 1):127–134. doi:10.1159/000481243
44. Okamoto T, Schlegel A, Scherer PE, Lisanti MP. Caveolins, a family of scaffolding proteins for organizing "preassembled signaling complexes" at the plasma membrane. *J Biol Chem*. 1998;273:5419–5422. doi:10.1074/jbc.273.10.5419
45. Filippini A, Sica G, D'Alessio A. The caveolar membrane system in endothelium: from cell signaling to vascular pathology. *J Cell Biochem*. 2018;119:5060–5071. doi:10.1002/jcb.26793
46. Castillo Bennett J, Silva P, Martinez S, Torres VA, Quest AFG. Hypoxia-induced caveolin-1 expression promotes migration and invasion of tumor cells. *Curr Mol Med*. 2018;18:199–206. doi:10.2174/1566524018666180926163218
47. Zhou Q, Peng X, Liu X, et al. FAT10 attenuates hypoxia-induced cardiomyocyte apoptosis by stabilizing caveolin-3. *J Mol Cell Cardiol*. 2018;116:115–124. doi:10.1016/j.yjmcc.2018.02.008